Identification and Analysis of the 1998 Central American Smoke Event at the ARM SGP CART Site

R. A. Peppler and C. P. Bahrmann
Cooperative Institute for Meoscale Meteorological Studies
University of Oklahoma
Norman, Oklahoma

L. Ashford
Oklahoma Department of Environmental Quality
Air Quality Division
Oklahoma City, Oklahoma

J. C. Barnard, N. S. Laulainen, and D. D. Turner
Pacific Northwest National Laboratory
Richland, Washington

R. A. Ferrare
National Aeronautics and Space Administration
Langley Research Center
Hampton, Virginia

R. N. Halthore
Brookhaven National Laboratory
Upton, New York

J. A. Ogren and P. J. Sheridan
National Oceanic and Atmospheric Administration
Climate Monitoring and Diagnostics Laboratory
Boulder, Colorado

M. R. Poellot
University of North Dakota
Grand Forks, North Dakota

M. E. Splitt
Cooperative Institute for Regional Prediction
University of Utah
Salt Lake City, Utah

Introduction

Drought-stricken areas of Mexico and Central America were victimized by forest and brush fires that burned out of control from mid-February into June 1998. Southerly and southwesterly flows at various times during this period helped transport smoke from this biomass burning over the Gulf of Mexico and into the eastern half of the United States, especially into southern and southeastern states. Visibility was greatly reduced from Texas to south Florida as a result of this smoke and haze. High levels of fine particulates were measured at some locations. State and national agencies, including the National Weather Service in Oklahoma on May 13, issued public health advisories and haze alerts.

This event was also detected over the Southern Great Plains (SGP) Cloud and Radiation Testbed (CART) site by the Atmospheric Radiation Measurement (ARM) Program's unique array of instrumentation and by sensors deployed by the Oklahoma Department of Environmental Quality (ODEQ) Air Quality Division. Data from these sensors suggest elevated levels of aerosol loading and ozone concentrations occurred over the CART site during part of May 1998. Analyses are shown here from the Raman Lidar, Aerosol Observing System (AOS), Solar and Infrared Radiation Stations (SIRS), Multi-Filter Rotating Shadowband Radiometer (MFRSR), Cimel Sunphotometer (CSPHOT), and a condensation nuclei (CN) counter on-board the University of North Dakota Citation aircraft. The Raman Lidar analyses demonstrate a new capability for retrieving aerosol extinction profiles.

Large-Scale Environment of the Smoke Event

Fire Locations

Geostationary Operational Environmental Satellite (GOES)-8 infrared (IR) and Advanced Very High Resolution Radiometer (AVHRR) channel 3 imagery (Cooperative Institute for Mesoscale Meteorological Studies [CIMSS], University of Wisconsin; National Oceanic and Atmospheric Administration/National Environmental Satellite, Data, and Information Service [NOAA/NESDIS]) helped identify "hot spots" (the fires) in Central American and Mexico. The widespread magnitude of these fires was quite evident in such images, particularly on the Yucatan Peninsula. Figure 1 shows the GOES-8 ABBA Experimental Fire Product for May 18.

Satellite Imagery of Smoke Pall

Enhanced visible and multichannel imagery (CIMSS, University of Wisconsin; NOAA/NESDIS) during May clearly defined the areal coverage of the smoke and haze. Figure 2 shows an example of the multi-channel imagery for May 14. Yellow-brown shading delineates smoke areas in this image.

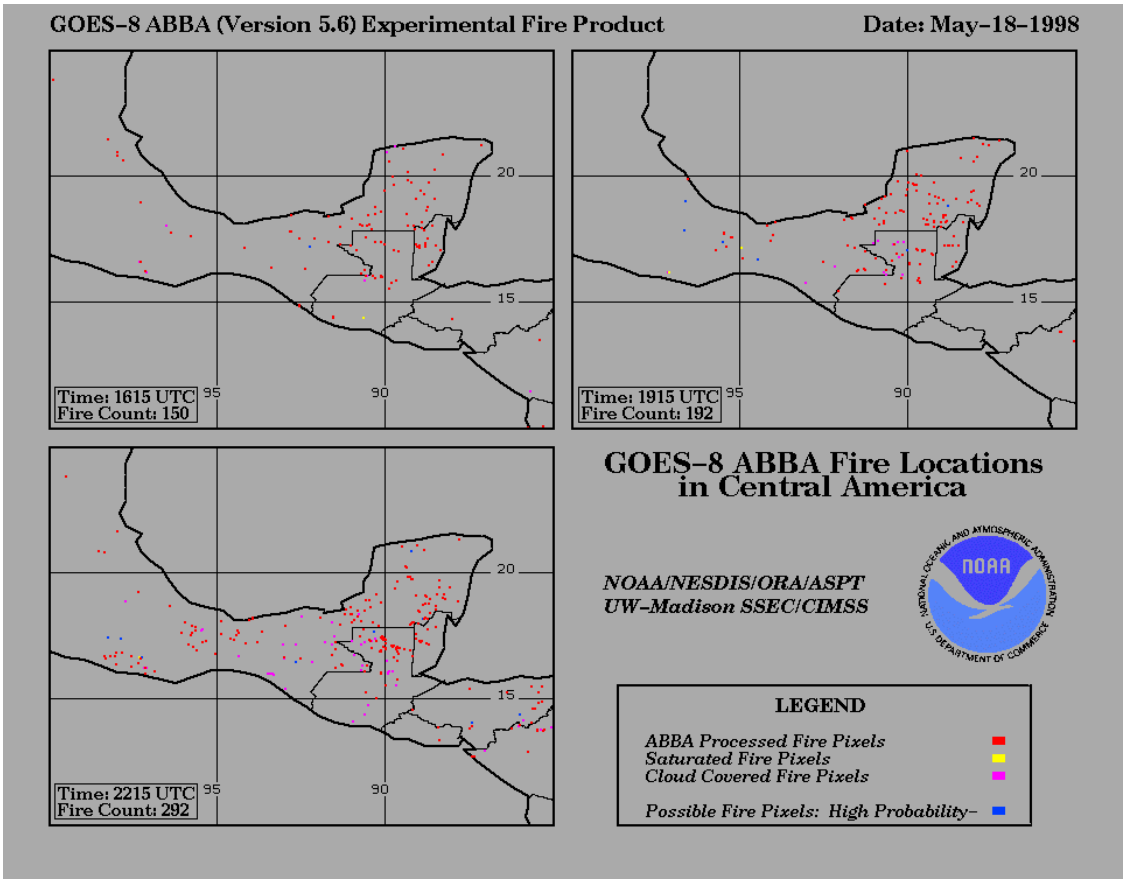

Figure 1. GOES-8 ABBA Experimental Fire Product showing locations of fires on May 18.

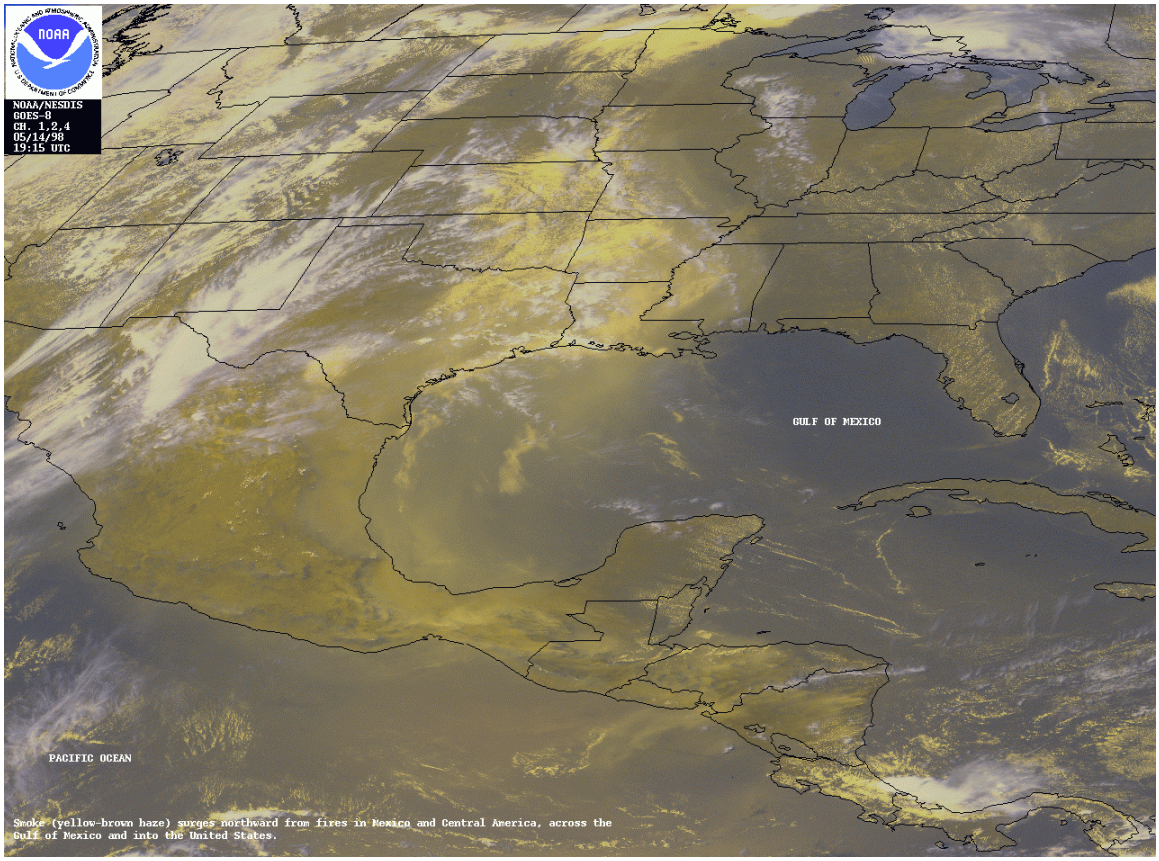

Figure 2. GOES multichannel image for May 14 showing smoke/haze areas.

Satellite Detection of Aerosols

The Total Ozone Mapping Experiment (TOMS) aerosol data product (National Aeronautics and Space Administration/Goddard Space Flight Center [NASA/GSFC]) contains measurements of ultraviolet (UV)-absorbing tropospheric aerosols and can be used to generate daily global maps of these particles. TOMS images represent smoke from a variety of ground-based sources such as biomass burning, whether naturally occurring or caused by agriculture, oil industry fires, or industrial smoke. It should be noted that it can be insensitive to aerosols in the lowest 1 to 2 kilometers of the atmosphere, but does allow a good overall view of the large-scale condition.

May 14 and 19 were the most active TOMS aerosol days over the CART region (Figure 3), with indices up to 1.7 over the eastern half of the CART on the 14th and also over all but the northwest corner of the CART on the 19th. The largest aerosol index (up to 1.7) over the central facility itself occurred on the 19th. A cold frontal passage early on the 15th cleared the skies of aerosols for the intervening period. Other days with TOMS aerosol indices of up to 1.2 occurred on May 9, 15, 17, and 25 in extreme southeastern Oklahoma; May 13, 18, and 23 in southern Oklahoma; May 20 (most of the eastern half of the CART site), May 21 (parts of the eastern and northwestern CART site), and May 22nd (northeastern Kansas).

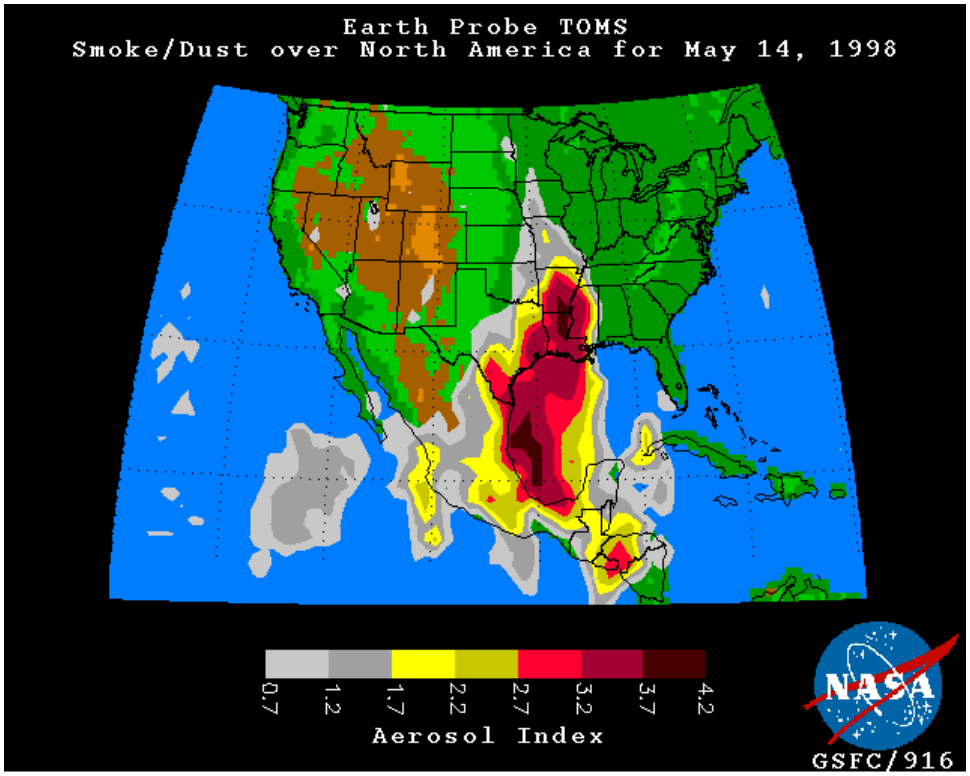

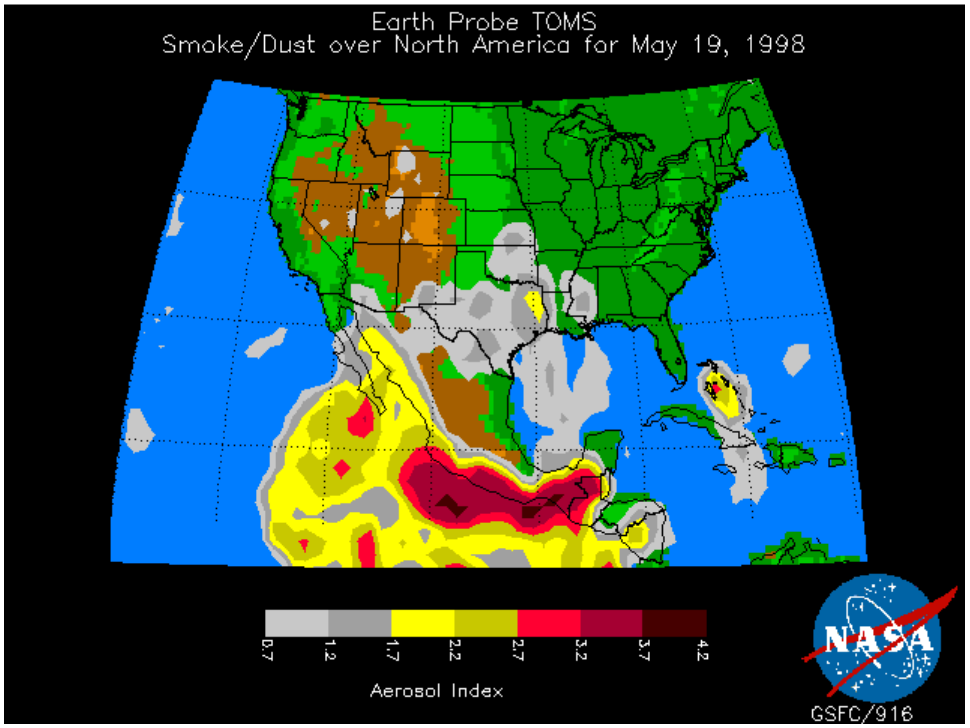

Figure 3. TOMS aerosol indices for May 14 and 19.

Trajectory Analyses

Backward trajectories were produced using software available on the NOAA Air Resources Laboratory HYSPLIT4 website: http://www.arl.noaa.gov/ready/hysplit4.html. Archived EDAS meteorological data were used as input. The latitude/longitude of the CART Raman Lidar was used as the ending point (36.61 degrees north/97.49 degrees west) and trajectories were computed backward in time up to 96 hours (4 days). Tick marks on the trajectory plots indicate 6-hour movement locations.

Trajectories ending at the central facility generally emanated from the north and west up until May 13/00 Universal Time Coordinates (UTC), except for May 6/00 UTC, when the 850 HPa trajectory came from the western Gulf northwest of the Yucatan. From May 12/12 UTC through the rest of the month, except after the cold-frontal passage (May 16/12 UTC-May 17/00 UTC) and May 24/00 UTC and May 29/00 UTC, at least one trajectory reaching the central facility (especially lower level ones such as 850, 900, or 950 HPa) began somewhere in the fire region. 700 HPa or higher trajectories generally came from the west or southwest, far west of the fire region. Particularly interesting smoke trajectories occurred on May 14/12 UTC-May 15/12 UTC (when 850 and 900 HPa trajectories started either on the Yucatan Peninsula, just west of it, or in adjacent Gulf of Mexico waters), May 18/12 UTC-May 19/00 UTC (850 and 900 HPa trajectories started on the Mexican coast just west of the Yucatan Peninsula or in adjacent Gulf of Mexico waters), and May 22/12 UTC-May 26/12 UTC (850, 900, and 950 HPa trajectories began anywhere from the eastern Mexican coast to the Yucatan Peninsula). Figure 4 shows backward trajectories for two of those periods, May 15/12 UTC and May 19/00 UTC.

Oklahoma Department of Environmental Quality/Air Quality Division Analyses

The Oklahoma Department of Environmental Quality (ODEQ), Air Quality Division, knew of the fires burning in Mexico on May 11, 1998, but forecast information indicated that the smoke plume would be well south of Oklahoma that day, so no impact was expected. Those expectations were correct for most pollutants; however, an increase in haze was perceptible that day. Later, it would be determined that the Division's particulate monitors recorded higher than normal values, but these values were not elevated enough to cause concern. Satellite imagery on May 11 had denoted a barely visible upside down V-shaped plume over Oklahoma. The abnormal amount of haze observed, and the satellite image, led the Division to believe that a shallow smoke-laden air mass moved north from Texas into Oklahoma on May 11.

The Division also detected high ozone readings from Oklahoma City area ozone monitors on May 11. Ozone concentrations are highly dependent on temperature and wind speed, so it was unusual that the ozone concentrations observed were as high as they were that day given that wind speeds were high and the temperatures relatively low, the opposite of what is expected. Table 1 lists, for each ozone-monitoring site in the Oklahoma City area, the days on which were recorded the ten highest 8-hour averages of ozone in 1998. Average wind speeds for the 8 hours, which coincide with the ozone readings and daily high temperature, are also listed. The values for each parameter were averaged for each of the ten days. It is apparent that wind and temperature conditions that accompanied the elevated ozone levels on May 11 were quite different from those of other days shown in the table, likely indicative of the shallow layer of smoke intrusion into central Oklahoma.

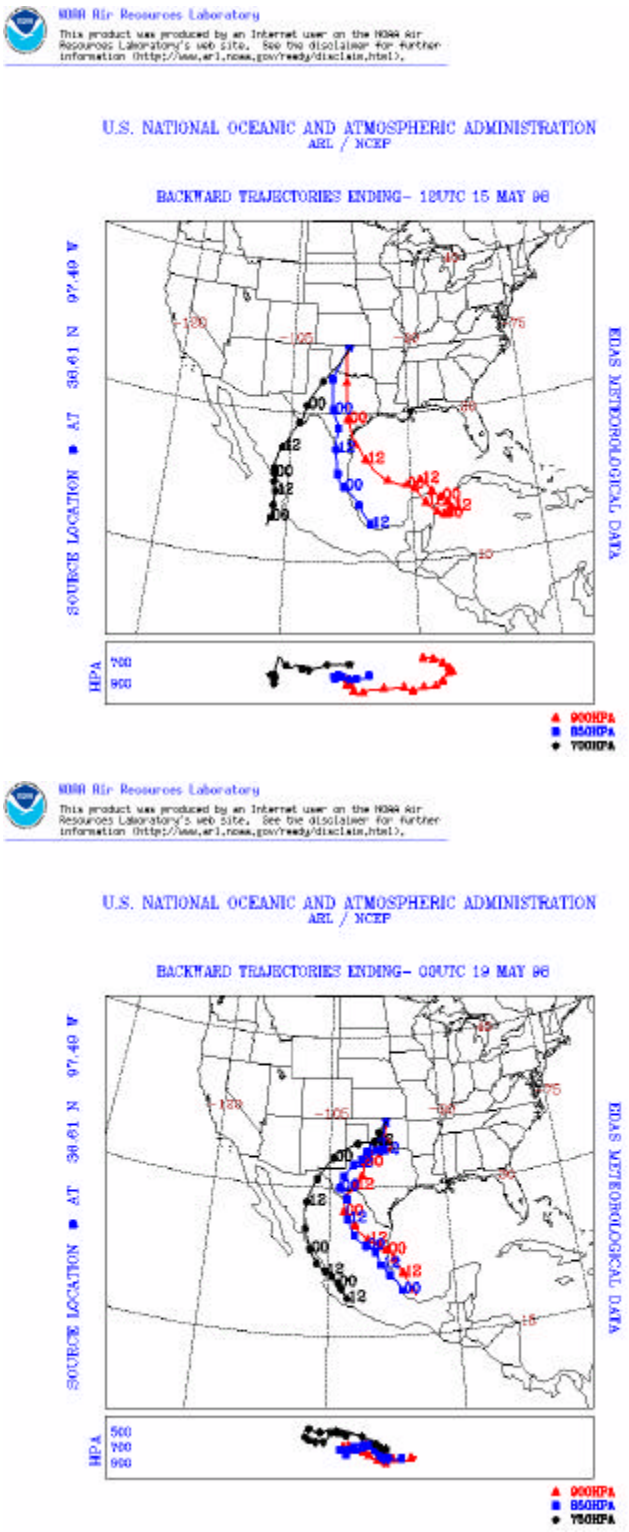

Figure 4. NOAA Air Resources Laboratory (ARL) backward trajectories ending at the SGP CART site on May 15/12 UTC and May 19/00 UTC.

Table 1. Ten highest 8-hour average ozone concentrations in central Oklahoma in 1998.

Site	1st	2nd	3rd	4th	5th	6th	7th	8th	9th	10th
Oklahoma City	0.125	0.096	0.92	0.09	0.089	0.086	0.084	0.083	0.082	0.081
Temperature	94	92	94	83	90	95	91	97	89	103
Wind Speed	0	2	1	12	1	2	2	8	6	9
Date	Sept. 5	Sept. 4	Sep. 1	May 11	Sept. 2	Sept. 7	Aug. 7	Sept. 6	Aug. 16	Sept. 9
(0.084)										
Edmond	0.109	0.093	0.091	0.088	0.084	0.084	0.084	0.083	0.082	0.082
Temperature	94	92	95	83	89	97	91	94	97	95
Wind Speed	0	2	2	12	6	8	5	0	3	3
Date	Sept. 5	Sept. 4	Sept. 7	May 11	Aug. 16	Sept. 6	Sept. 29	Sept. 1	Aug. 1	Aug. 20
(0.084)										
Moore	0.106	0.097	0.093	0.093	0.086	0.084	0.082	0.082	0.08	0.079
Temperature	94	92	90	83	95	97	87	103	89	94
Wind Speed	0	2	1	12	8	8	3	8	6	1
Date	Sept. 5	Sept. 4	Sept. 2	May 11	Sept. 8	Sept. 6	Aug. 15	Sept. 9	Aug. 16	May 1
(0.084)										
Goldsby	0.102	0.094	0.088	0.087	0.085	0.084	0.084	0.083	0.079	0.078
Temperature	90	92	94	83	95	94	89	97	103	78
Wind Speed	1	2	0	12	8	1	6	8	8	16
Date	Sept. 2	Sept. 4	Sept. 5	May 11	Sept. 8	May 1	Aug. 16	Sept. 6	Sept. 8	April 24
(0.084)										
Average Concentration	0.111	0.095	0.091	0.090	0.086	0.085	0.084	0.083	0.081	0.080
Average Wind Speed	0.3	2.0	1.0	12.0	5.8	4.8	4.0	6.0	5.8	7.0
Average Maximum Temperature	93.0	92.0	93.3	83.0	92.3	95.8	89.5	97.8	94.5	92.5

ARM SGP CART Site Analyses

Aerosol Observing System

Unusually high aerosol concentrations were measured by the Aerosol Observing System (AOS) at the central facility during May. The concentrations observed were thickest around May 14, but high aerosol loadings were observed on other days as well. Ozone levels exceeded 80 ppbv on seven days during the period May 5-25, but did not vary day-to-day nearly as much as the aerosol levels. The annual average aerosol light scattering coefficient at the central facility is about 25 Mm-1, but peak levels of over 600 Mm-1 were observed in mid-May. These values correspond to visibilities of about 60 miles and 4 miles, respectively.

Figure 5 shows aerosol total light-scattering coefficient (Bsp) in the green, red, and blue channels and aerosol light absorption coefficient (Bap) in the green channel. These coefficients showed peaks around May 14 and 18. A dramatic drop off in these coefficients around 12 UTC on May 15 is clearly evident and was associated with the cold frontal passage and minor rain event. A subsequent return to higher than average scattering and absorption coefficients began on May 17. This return to higher values was associated with the surface winds returning to a southerly direction, reintroducing the area to the smoke-polluted air mass. Associated aerosol number concentration and single-scatter albedo values (not shown) illustrated similar patterns as Bsp and Bap.

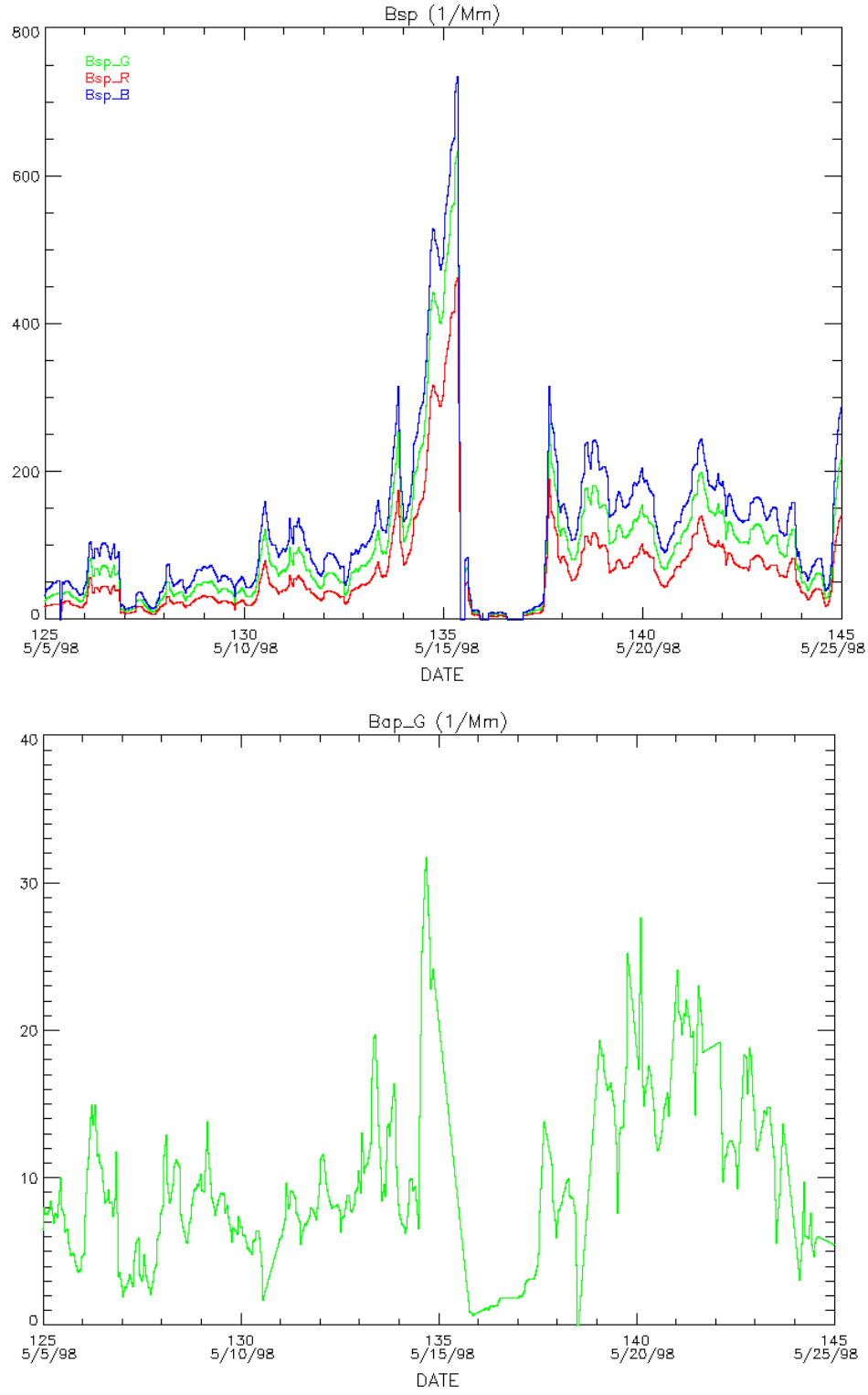

Figure 5. Aerosol total light-scatttering coefficient (Bsp) in the green, red, and blue channels and aerosol light absorption coefficient (Bap) in the green channel for May 1998.

Raman Lidar

The ARM SGP CART Raman Lidar, which autonomously measures profiles of water vapor, aerosols, and clouds, observed high values of aerosol extinction during May 13-14 and May 18-20 when smoke was present over the SGP site. Vertical distributions of aerosol extinction, water vapor mixing ratio, relative humidity, clouds, and depolarization over the SGP site during May 13-20 were analyzed using the SGP Raman Lidar data (Figure 6). Relative humidity profiles were computed using the Raman Lidar water vapor mixing ratio profiles and temperature profiles derived from a physical retrieval algorithm that uses data from a collocated Atmospheric Emitted Radiance Interferometer (AERI) and GOES. Wayne Feltz (University of Wisconsin) provided these temperature profiles. By integrating the aerosol extinction profiles between the surface and 6 km, estimates of the aerosol optical thickness (AOT) were derived from the SGP Raman Lidar data (Figure 6). Similarly, estimates of the precipitable water vapor (PWV) were obtained by integrating the Raman Lidar profiles of water vapor mixing ratio with altitude (Figure 6).

As can be seen from the aerosol extinction image (Figure 6, top left), the SGP Raman Lidar observed large values of aerosol extinction in the lowest 2 km on May 13-14, followed by very low values during the latter part of May 15 and on May 16. The rapid drop in aerosol extinction measured by the Raman Lidar matches well the similar decrease in aerosol light scattering measured at the surface by the AOS discussed above. Beginning on May 17 and continuing through May 20, the Raman Lidar measurements revealed high aerosol extinction values extending through a large (0-6 km) region of the troposphere. The trajectory analyses described above support the transport of smoke throughout a large region of the troposphere at this time. The change in the vertical distribution of aerosols between May 14 and May 19 may have a significant impact on the TOMS aerosol retrievals and is the subject of further investigations. The Raman Lidar measurements of AOT (Figure 6, top right) show the large variability of aerosol loading during this period and show peak values of AOT occurred on May 19. The Raman Lidar AOT measurements compare favorably with those measured by the SGP Cimel Sunphotometer (see Figure 9).

The Lidar data also showed clouds (Figure 6, middle right) were often located at the top of the aerosol layers. The locations of clouds during this period were derived from the Raman Lidar aerosol and depolarization data (Figure 6, middle left). On May 14, the clouds below 2 km observed by the Lidar were located just above the region of very high aerosol extinction. In slight contrast to this, on May 17-20, there were fewer boundary layer clouds and the aerosols were spread over a much larger altitude region. The Lidar data also show the presence of mid and high level clouds during much of the period. The surface AOS data show good correlations between aerosol scattering and concentrations measured at the surface and the Lidar aerosol extinction measurements.

The Raman Lidar water vapor shows the presence of relatively moist conditions in the lowest 2 km until mid-day on May 15. Increasing moisture on May 17, which continued through May 20, followed the rapid decrease in moisture on May 16. As in the case of aerosol extinction, the relatively high water vapor amounts were spread over a large altitude region. The relative humidity and water vapor mixing ratios (Figure 6, bottom left and right, respectively), as well as the aerosol optical thickness and precipitable water vapor, showed the high correlation between water vapor and aerosol extinction that existed

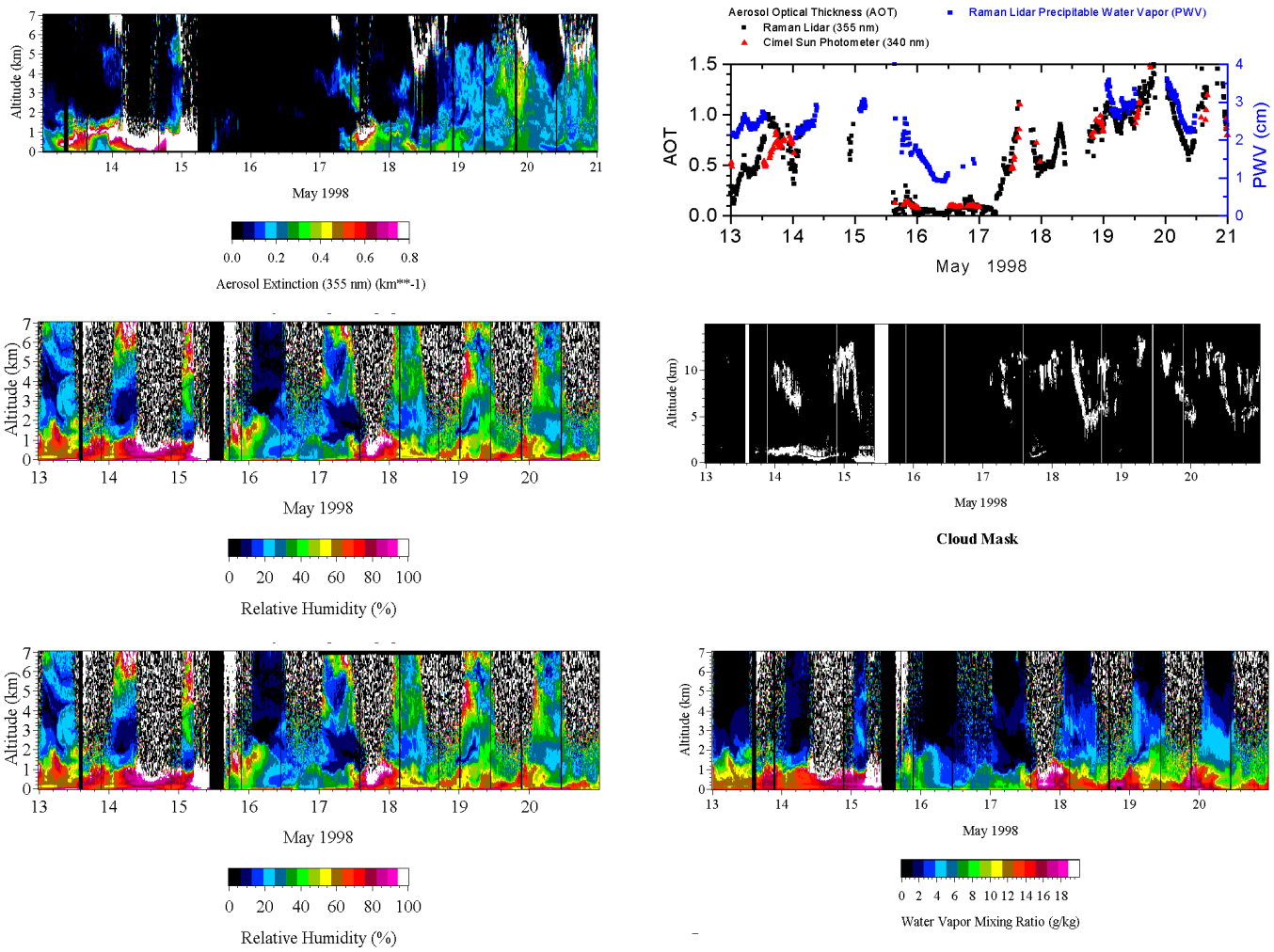

Figure 6. SGP Raman Lidar analyses for May 13-20; aerosol extinction and aerosol optical thickness/precipitable water vapor (top); depolarization ratio and cloud mask (middle); relative humidity and water vapor mixing ratio (bottom).

throughout this period. The white speckled areas in the water vapor mixing ratio and relative humidity images are due to increased noise in the daytime, when background skylight reduces the maximum altitude range for water vapor retrievals. This correlation is due both to the air mass properties as well as the hygroscopic nature of the aerosols.

Solar and Infrared Radiation Stations

Dust related events have been shown to affect the broadband solar radiation by decreasing the direct component of the insolation and increasing the diffuse component. The Asian Dust Storm of 1998 was shown to have this effect in the northwestern United States (see on-line report at *http://solardat.uoregon.edu/html/98_china_dust_cloud.html*). A similar approach was taken here to identify the impact of the Central American fires on the broadband radiation data over the SGP.

Clearness indices are generally defined as the ratio of the total solar radiation observed at the ground (Hg) and a clear-sky total radiation at that location (Ho), for example, extraterrestrial radiation. The clearness index (K) is simply Hg/Ho (see Black et al. 1954). Several variants of the clearness index were used in this study to better discriminate between effects of aerosol and that of water vapor on the total solar radiation: H0 extraterrestrial estimate; H1 extraterrestrial estimate with an air mass correction; H2 clear-sky model with no water vapor; H3 clear-sky model with water vapor based on microwave radiometer; and H4 clear-sky model with water vapor based on surface dew point.

The clear-sky model was based on Myers and Dale (1983). It includes simple treatment of aerosol and water vapor effects on the observed total solar radiation. The clearness index was then calculated using the observed total solar radiation and each of the five estimates above. The indices were only calculated under conditions that were determined to be cloud-free by observation of the radiation data (and use of satellite data for some of the data from May 1998). All estimates were based on values near solar noon. The clear-sky indices were calculated (when possible) during May 1997 for reference and for May 1998 for the SIRS radiometers at E13 (the central facility).

In addition, to assess the change in partitioning of the solar radiation into direct and diffuse components, ratios of the diffuse solar radiation to that of the total solar radiation were calculated (using data from the SIRS shaded and unshaded pyranometers). These ratios were calculated for May 1997 and May 1998 at E13, and for May 1998 at E25 (located in southeastern Oklahoma).

Figure 7 depicts the temporal variation of the clearness indices and the spatial variation of the diffuse/total ratios during the month. In general, the clear-sky indices indicated less attenuation of solar radiation in May 1998 than in 1997 for comparable periods, which was not anticipated. But, a noticeable dip in the indices is noted on May 13, followed by a strong jump in the indices by May 15. Based on the satellite image references in this report, it is assumed that fire-related aerosols had advected over the central facility by the 13th via southerly surface winds, but were quickly advected out of the region by a storm system, which brought in a drier and cleaner air mass from the northwest by the 15th. The fluctuations in the clearness indices are viewed to be largely as a result of change in aerosol content in the atmosphere since each of the indices show the same variations whether or not they included some kind of treatment of water vapor effects. Lower index values were also noted later in the month of May 1998, but the observations are sparse enough and fairly late in the haze event that a clear assessment of this later period is not currently available. It is quite likely that the smoke related aerosols had circulated back into north central Oklahoma following the clearing event on the 15th. The spatial variability of the average diffuse/total ratio over a 10-minute period at 1830 UTC (near solar noon) across the CART site on May 13. Slightly different data times were used for some of the sites since they experienced cloudiness at 1830 UTC (EF7, EF10, EF20, EF22, and EF24). This analysis shows a northwest to southeast gradient in the ratios, which likely is correlated with the fire-related aerosol loading. There also appears to be some mesoscale variability in the pattern.

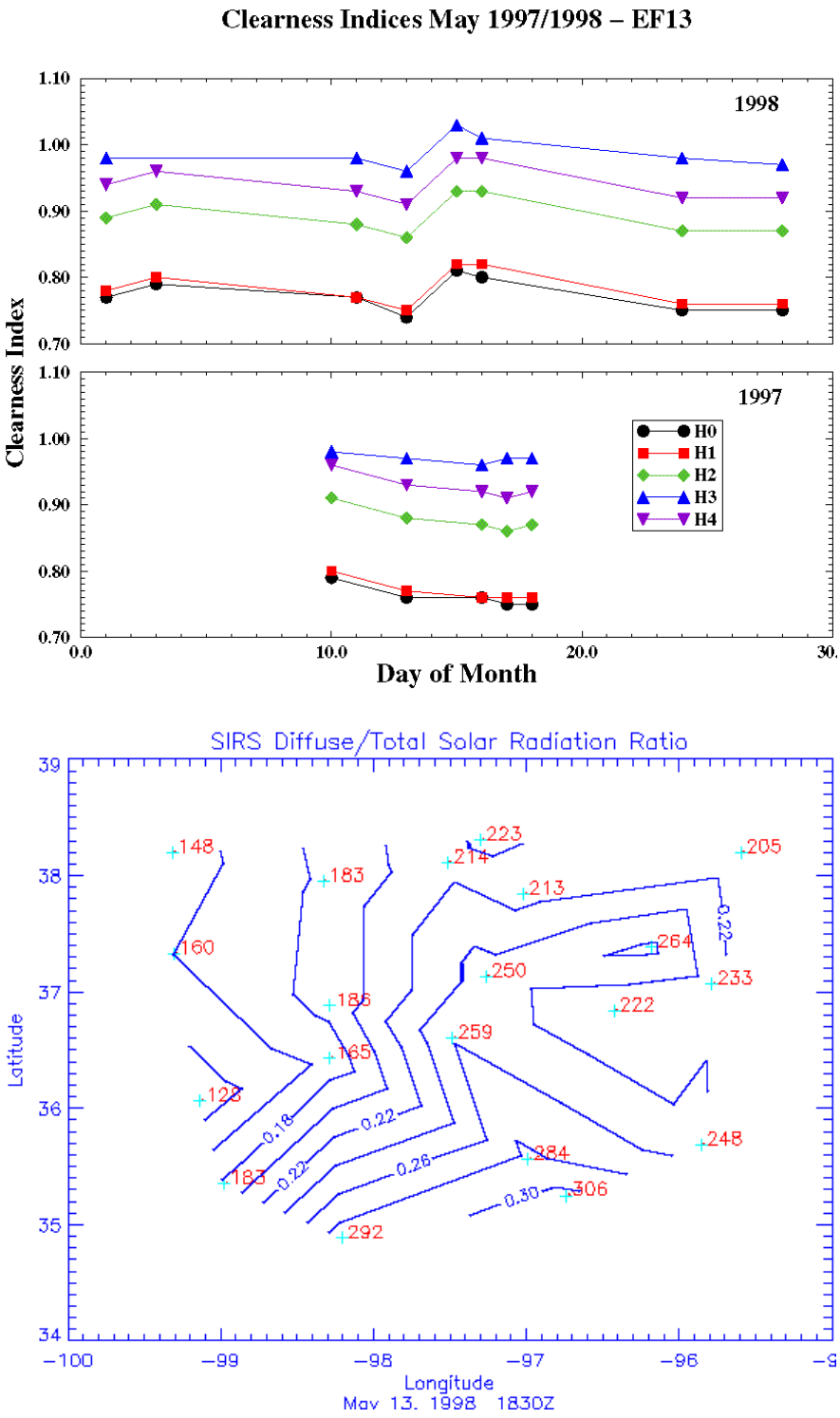

Figure 7. SIRS clearness indices for May 1998 and diffuse/total ratios for May 13 at 1830 UTC.

Multi-Filter Rotating Shadowband Radiometer

Figure 8 displays MFRSR-derived AOT from the SGP central facility. AOT were obtained by subtracting the Rayleigh scattering optical thickness and ozone optical thickness from the total optical thickness, as determined from the Beer-Lambert-Bouguer law and an assumed calibration constant for each wavelength channel. A mean ozone column of 300 Dobson units was used for the ozone correction. Data are daily averages over periods where there was no cloud interference, as judged from an inspection of the temporal variability of AOT and the wavelength exponent of AOT. Day 121 corresponds to May 1. The data show an overall gradual increase in AOT until May 13, followed by an abrupt increase on May 14. AOT decreased to near background levels as a result of a frontal passage on May 15. Following frontal passage, AOTs were abnormally high for about a week, with a peak on May 19. Values of AOT had returned to normal conditions by the first of June. The wavelength exponent of AOT decreased from normal values of 1 to 1.1 to about 0.5 during the peak of the smoke event, indicating a shift to larger particle sizes, indicative of well aged aerosol. The AOT values during the peak of the smoke event may have some contamination from clouds, since both the smoke plume and clouds could exhibit considerable temporal variability.

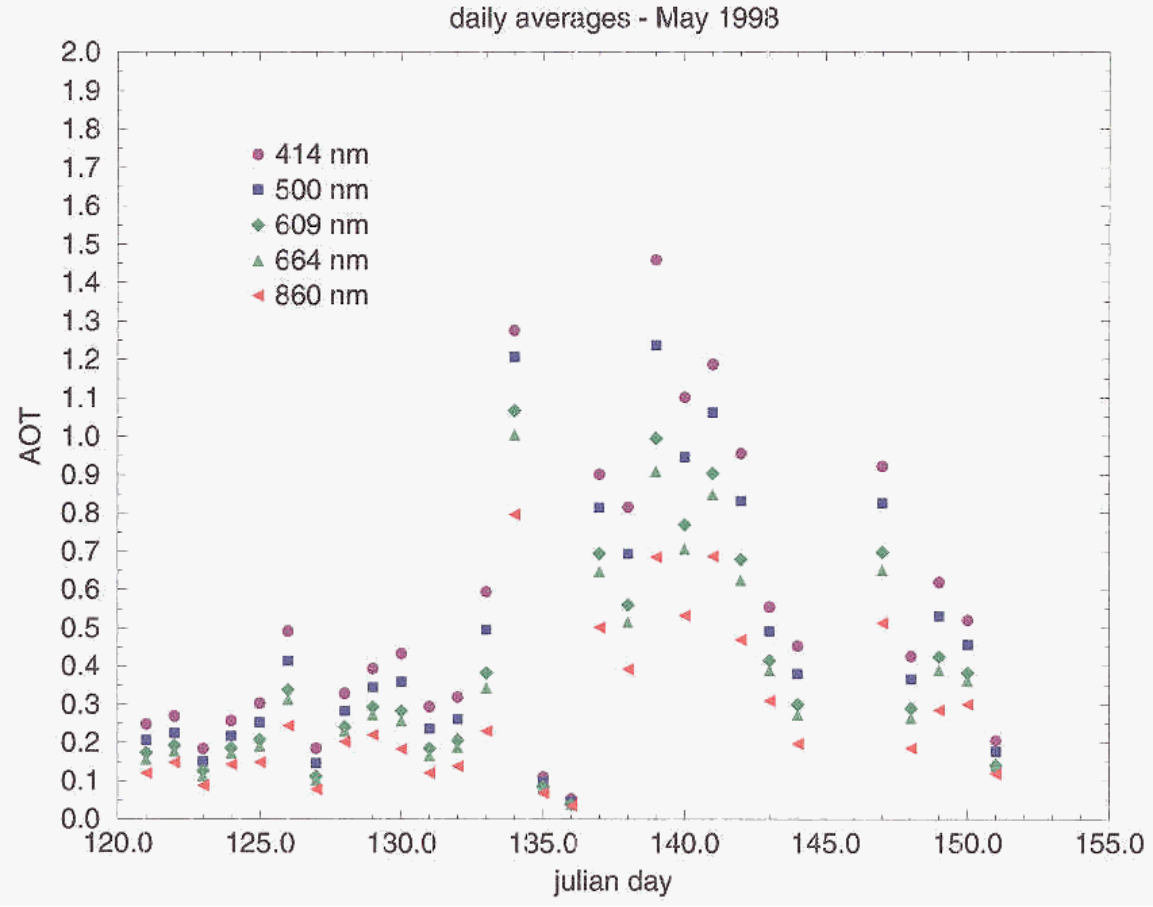

Figure 8. MFRSR AOT for five channels in May 1998.

Cimel Sunphotometer

Daily averages of AOT derived from the CSPHOT in Figure 9 show that values peaked in particular on May 14, 19, 21, and 27. Also noticeable is the sharp drop experienced on May 15 and 16 after the frontal passage. The high values found are unusually high and are not typical of northern Oklahoma. The low values recorded are probably representative of the background. Interestingly, the Angstrom exponent (see Figure 9) was near or above 1.0 most of the time. Smoke is made of very small particles that tend to have a high Angstrom exponent. Admittedly, there was likely some mixing with "regular" aerosols along the path from Central America to the CART site, which might explain why Angstrom values are not much above 1.0.

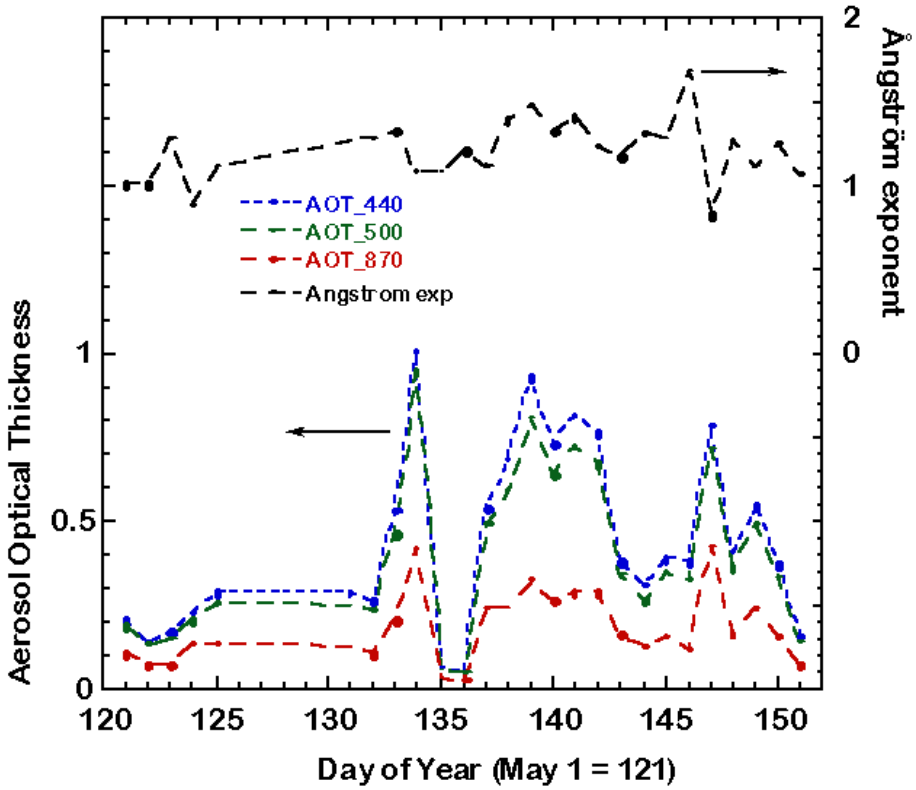

Figure 9. AOT and Angstrom coefficients from the Cimel Sunphotometer for May 1998.

University of North Dakota Citation Condensation Nuclei Counter

The University of North Dakota Citation made overflights of the SGP CART site for the ARM Program as part of a Cloud Physics Intensive Observation Period (IOP) that was conducted from April 27 through May 17, 1998. In addition to carrying a wide array of cloud physics instrumentation, the Citation was also equipped with a CN counter. Flights were made on April 29 and May 1, 2, 8, and 14. Two summary images have been produced showing data collected by the Citation's CN counter, and are shown in Figure 10. The left image shows the vertical profiles of CN concentrations in the lowest

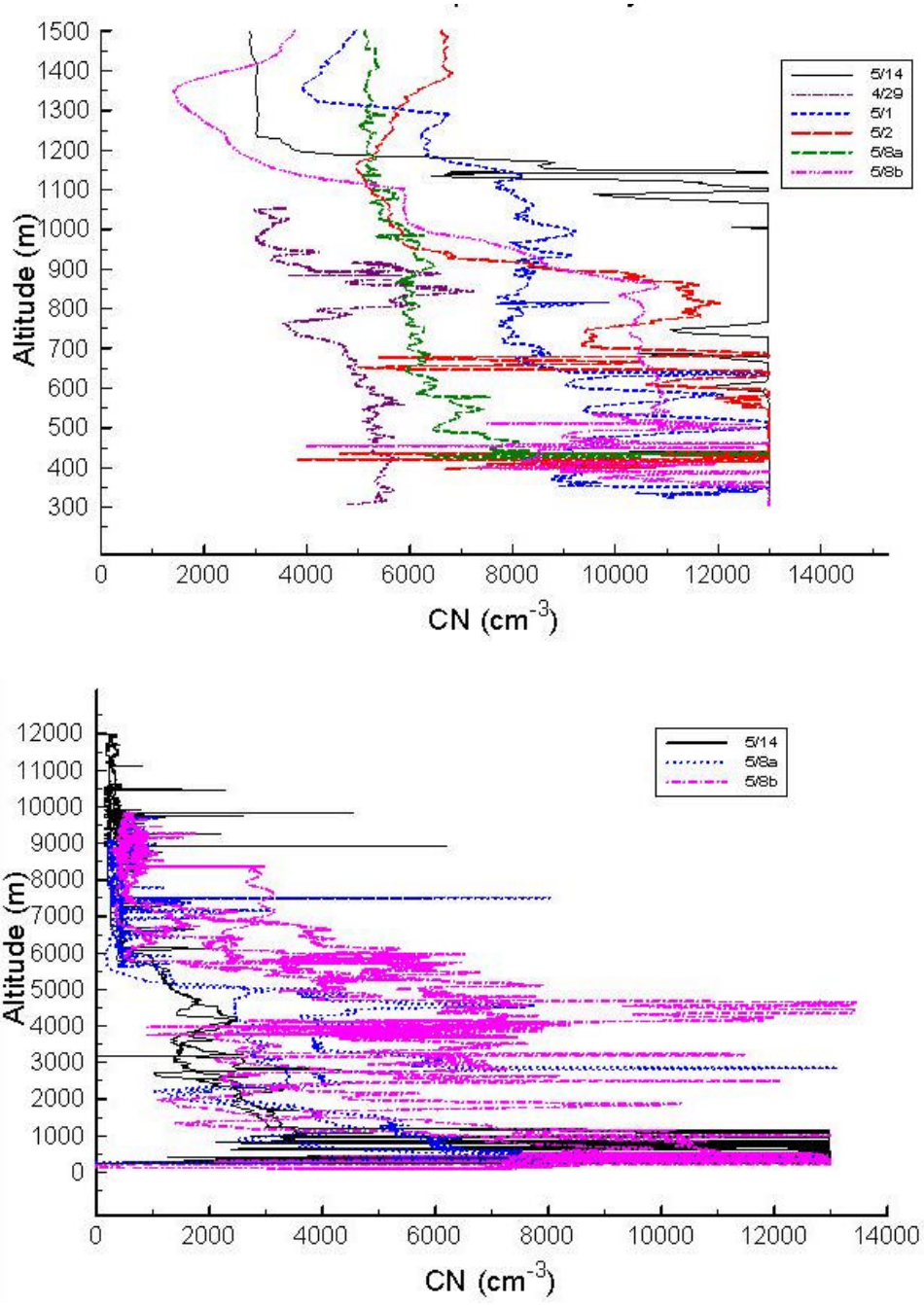

Figure 10. CN profiles as measured in-situ by the North Dakota Citation for flights in April-May 1998.

1500 meters for all of the 1998 IOP flights, while the right image shows profiles through the full altitude range for three of the flights (two flights on May 8 and another on May 14). These were obtained during descent back into the Ponca City airport. The CN counter is a TSI 3760, which counts essentially all particles from about 0.01 to 3 microns. In the left image, the aerosols on May 14 saturated the CN counter below 1200 meters, which was probably the top of the boundary layer. Occasional saturation

can also be seen from the data of several other flights. This condition seemed to cause the CN readings to spike downward toward relatively low values. These spikes were removed from the curve for the 14th to clean up the graph, but were left in for the others. While it is unfortunate that the CN counter did saturate, these data still show how the boundary layer filled with the smoke aerosol. They also show the magnitude and structure of the CN distribution for the other flights. Of interest in the right image is the elevated CN values in the 3 km to 6 km layer, which increased dramatically from the start of the first flight on May 8 (the left-hand blue curve), or around 1500 UTC, to the time of the second flight, about 2000 UTC to 2300 UTC. It is not certain that this phenomenon was due to the Central American smoke, but trajectories calculated by the NOAA ARL for air parcels starting early on May 7 west of the Yucatan Peninsula did cross into Oklahoma at the 850 HPa and 750 HPa levels on May 9 and 10.

References

Black, J. N., C. W. Bonython, and J. A. Prescott, 1954: Solar radiation and the duration of sunshine. *Quarterly Journal of the Royal Meteorological Society*, **80**, 231-235.

Myers, T. P., and R. F. Dale, 1983: Predicting daily insolation with hourly cloud height and coverage. *Journal of Climate and Applied Meteorology*, **22**, 537-545.